

## Article

# Effect of Seawater Environment on the Structure and Performance of Basalt Continuous Fiber

Qingwei Wang <sup>1,2</sup> , Tan Yan <sup>1,2</sup> and Linfeng Ding <sup>1,2,\*</sup>

<sup>1</sup> State Key Laboratory of Modification of Fiber Materials, Shanghai 201620, China; wqwq888@dhu.edu.cn (Q.W.); 2190330@mail.dhu.edu.cn (T.Y.)

<sup>2</sup> Engineering Center of Advanced Glass Manufacturing Technology, Ministry of Education, Donghua University, Shanghai 201620, China

\* Correspondence: linfeng.ding@dhu.edu.cn

**Abstract:** Basalt continuous fibers (BFs) have been widely applied in the construction industry including marine applications, however, the corrosion mechanism of BFs in a seawater environment is still not well understood. In this work, we explored the effect of the seawater environment on the weight loss, tensile strength, surface morphology, and microstructure structure of BFs via soaking the BFs in seawater solutions at different temperatures and durations. Results show that the weight loss ratio of BFs decreases at the first stage (around 18 h) of soaking at 80 °C, 85 °C, and 90 °C and then increases for longer soaking durations, while the tensile strength has the opposite change. This enhancement of tensile strength and chemical resistance (at the first stage of seawater soaking) is dominated by the ion-exchange induced ‘blunting’ mechanism, even though the results from a Fourier transform infrared (FT-IR) spectrometer and energy-dispersive spectroscopy (EDS) revealed the damaging of the Si–O–Si tetrahedral structure during the corrosion process. This work revealed the full corrosion process and corresponding mechanism of BFs in a seawater environment.

**Keywords:** basalt fiber; seawater environment; chemical durability; tensile strength; microcrack blunting



**Citation:** Wang, Q.; Yan, T.; Ding, L. Effect of Seawater Environment on the Structure and Performance of Basalt Continuous Fiber. *Materials* **2021**, *14*, 1862. <https://doi.org/10.3390/ma14081862>

Academic Editor: F. Pacheco Torgal

Received: 11 March 2021

Accepted: 7 April 2021

Published: 9 April 2021

**Publisher’s Note:** MDPI stays neutral with regard to jurisdictional claims in published maps and institutional affiliations.



**Copyright:** © 2021 by the authors. Licensee MDPI, Basel, Switzerland. This article is an open access article distributed under the terms and conditions of the Creative Commons Attribution (CC BY) license (<https://creativecommons.org/licenses/by/4.0/>).

## 1. Introduction

Basalt fiber (BF) is made by continuously drawing from a platinum-rhodium alloy bushing plate [1,2] where the pure basalt rocks are melting at around 1300–1500 °C. Compared with other inorganic fiber materials such as ordinary glass fiber and mineral wool fiber, basalt fiber has good high-temperature resistance and corrosion durability [3–6], and a similar composition to natural soil, so it has been widely used in reinforced construction materials to improve the mechanical properties and chemical stability of construction [7,8].

A large number of studies [9,10] show that basalt fiber-reinforced polymer reinforcement (BFRP) has good resistance to seawater erosion, and is expected to become an ideal alternative to traditional steel bars. The application of BFRP has the potential to solve the problem of severe corrosion and short service life of marine constructions. Many factors can affect the performance of BFRP in the marine environment, e.g., climate, exposure time, reinforcement method [11], and temperature [12]. Compared with the dry and wet cycle marine environment, the corrosion of BFRP in the immersion environment is much more serious. The increase of ambient temperature will also enhance the degradation and geometric deformation [13] of BFRP rods. Among these, the destruction of the interface between basalt fiber and epoxy resin matrix is the main reason for the degradation of the BFRP sheet [14]. The reaction of Fe<sup>2+</sup> in basalt fiber with Cl<sup>-</sup> in seawater, after it is exposed to seawater will accelerate the degradation of BFRP [15]. Moreover, the precipitation of salt will also accelerate the debonding of the fiber–matrix interface, and the hydrolysis of the epoxy resin matrix produces a large number of voids, which accelerates the degradation of the BFRP sheet [16].

Recently, many efforts have been made to improve the durability of BFRP in seawater. Among these, adding nanomaterials, e.g., silanized montmorillonite (Si-MMT) [17], nanotubes (HNTs) [18], etc., to the polymer matrix is one option that can improve the interface interaction between the BF and the polymer matrix, thereby increasing the bonding strength between the enhanced interface [19]. These studies were mostly focused on BFRP composite materials, however, and the performance of BF is also critical especially after the destruction or degradation of BFRP. Few works have examined directly the mechanisms of corrosion of BF in a seawater environment.

In this work, the effect of seawater environment on the surface morphology, structure, and mechanical properties of BFs is explored via immersing basalt fibers in seawater solutions. The mechanism of seawater corrosion on BFs was studied.

## 2. Experiment

### 2.1. Sample Preparation

The basalt fibers (BFs) were prepared by using basalt rocks from Shandong Province (Jiangsu Tianlong Continuous Basalt Fiber Co. Ltd., Yizheng, Jiangsu, China). The basalt rock was placed in a quartz crucible, heated to 1550 °C at a heating rate of ~600 °C/h in a high-temperature furnace, with an isothermal hold for 2 h. Then, the molten basalt melt was rapidly quenched in water to get the basalt glass. The chemical composition of basalt glass (determined by X-ray fluorescence analysis) is shown in Table 1.

**Table 1.** Chemical composition of basalt glass.

Composition	SiO <sub>2</sub>	Al <sub>2</sub> O <sub>3</sub>	Fe <sub>2</sub> O <sub>3</sub>	MgO	CaO	K <sub>2</sub> O	Na <sub>2</sub> O	Others
Content (wt%)	54.90	16.40	9.20	5.60	8.10	0.55	3.30	1.95

Lastly, the continuous BFs were prepared by using a laboratory monofilament fiber drawing system [20] with a platinum crucible at temperatures of ~1350 ± 10 °C and a take-up reel at a rotation speed of ~200 rpm.

### 2.2. Characterization

The seawater solution was prepared based on the ASTM D1141-98 (2013) [21] to simulate the marine environment. The composition is shown in Table 2 to create a seawater corrosion environment for aging experiments.

**Table 2.** Chemical composition of the seawater solution.

Composition	NaCl	MgCl <sub>2</sub>	Na <sub>2</sub> SO <sub>4</sub>	CaCl <sub>2</sub>	KCl
Content (g/L)	24.53	5.20	4.09	1.16	0.69

The accelerated aging method [22] was adopted in the whole process, where the seawater solution was heated to 80–90 °C to accelerate the aging rate of basalt fiber. The whole seawater aging process can be presented as follows: first, the BFs samples were dried at 100 °C for 2 h (h) before weighed and put into three glass beakers (0.1 g each); Then, the seawater solution was poured into the glass beakers to ensure that the BF samples were completely immersed in the seawater solution; then, the glass beakers were sealed with plastic wraps and fixed with rubber bands; finally, the glass beakers were placed into three ovens at temperatures of 80 °C, 85 °C, and 90 °C to start the aging experiment.

The weight loss of the BFs sample was measured after the aging experiment was processed for 6 h, 12 h, 18 h, 24 h, and 168 h (7 days). The BF samples were washed with distilled water 5 times and dried at 100 °C for 2 h before weighing in an analytical balance (Precisa, Zurich, Switzerland, ±0.0001 g). Meanwhile, a 1 mL seawater solution was also tested by inductively coupled plasma spectroscopy (ICP, Prodigy, Hudson, NH, USA).

The tensile strength of basalt fiber was tested by an electronic single fiber dynamometer (YG005A, Wenzhou, China) and 20 samples with diameters of about  $22 \pm 2 \mu\text{m}$  were taken from each group to test the tensile strength. A single filament BF sample with a length of  $20 \pm 1 \text{ mm}$  was fixed at the dynamometer and then stretching uniaxially at a speed of  $5 \text{ mm/min}$  until failure. The tensile strength ( $S$ , MPa) is calculated based on:

$$S = 10000F / \left( \frac{\pi}{4} d^2 \right) \quad (1)$$

where  $F$  is the failure strength in cN and  $d$  is the diameter of BF in  $\mu\text{m}$ .

The morphology and surface composition of the BFs before and after the aging experiment were measured by a field-emission scanning electron microscope (SEM, JSM-7500F, Tokyo, Japan) assisted with energy-dispersive spectroscopy (EDS). The microstructure of BFs after seawater aging was characterized by a Fourier transform infrared spectrometer (FT-IR, Nicolet 8700, Madison, WI, USA).

### 3. Result and Analysis

#### 3.1. Weight-Loss Ratio

The weight-loss ratio (mass loss divided by the initial mass) of BFs after soaking in seawater solution for up to 168 h at  $80^\circ\text{C}$ ,  $85^\circ\text{C}$  and  $90^\circ\text{C}$  is shown in Figure 1. In general, the overall weight-loss rate of BFs increases with the increasing temperature of seawater solution from  $80^\circ\text{C}$  to  $90^\circ\text{C}$  and exhibits a similar trend as a function of soaking time. In particular, the mass loss rate of BFs decreases gradually at the first 18 h and starts to increase afterward. For example, the weight-loss rate of the BFs sample after soaking at  $85^\circ\text{C}$  seawater solution for 18 h is only 0.42%, but that of the fiber at the same conditions for 24 h increases to 0.87% and it further increases to 2.26% at 168 h.

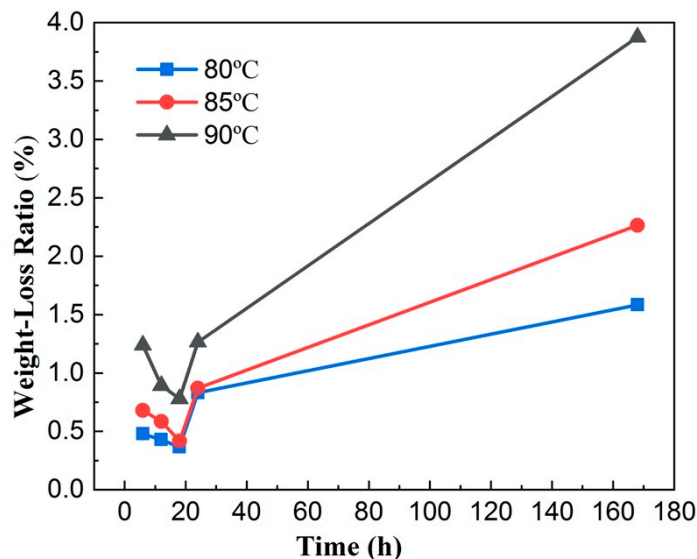
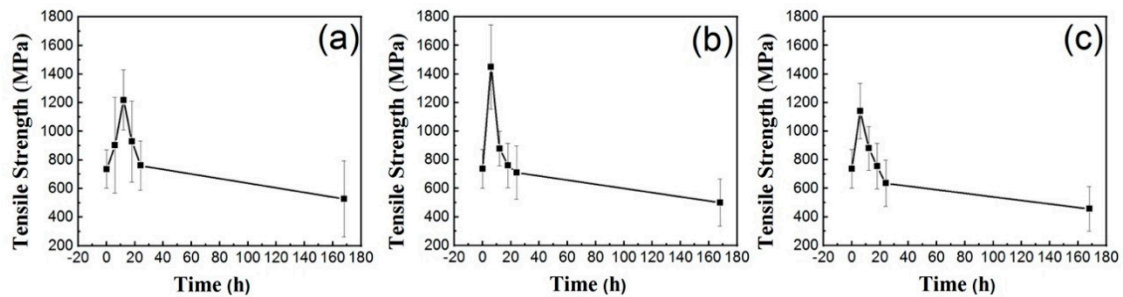


**Figure 1.** Weight-loss ratio of basalt fiber after soaking in seawater solution for 168 h at  $80^\circ\text{C}$ ,  $85^\circ\text{C}$ , and  $90^\circ\text{C}$ . The error bars are within the size of symbols.

#### 3.2. Tensile Strength

The tensile strength of BFs was measured and calculated according to the ISO 11566–1996 standard [23], which is the maximum strength the fiber can withstand before breakage. The tensile strength of basalt fiber after soaking at  $80^\circ\text{C}$ ,  $85^\circ\text{C}$ ,  $90^\circ\text{C}$  for 0, 6, 12, 18, 24, and 168 h is presented in Figure 2. Results from Figure 2a show that the tensile strength of BFs was continuously increased from 736 MPa to 1219 MPa during the first 12 h after soaking in the seawater solution, and it reduced gradually afterward. A similar phenomenon was detected also in Figure 2b,c, although the maximum tensile strength was reached slightly

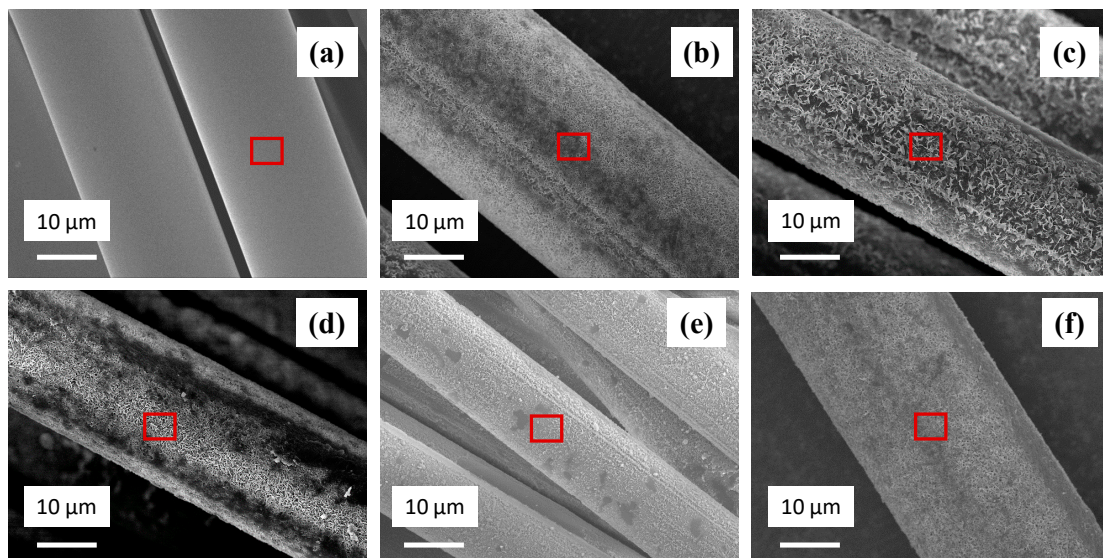
earlier at 6 h. The tensile strength of BFs will eventually decline to a very low level around 400 MPa after 168 h of soaking at different temperatures.



**Figure 2.** The tensile strength of basalt fiber immersed in seawater solution at different temperatures (a) 80 °C; (b) 85 °C; (c) 90 °C.

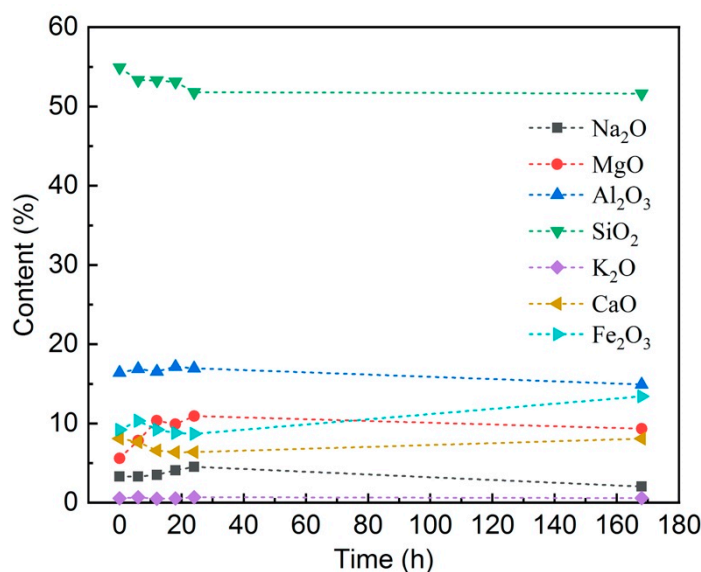
### 3.3. Scanning Electron Microscopy (SEM) and Energy-Dispersive X-Ray Spectroscopy (EDS)

Figure 3 shows the SEM surface morphology of pristine BFs and basalt fibers after they were immersed in seawater solution for different periods at 85 °C (biggest change in tensile strength). From the visual observation, the surface of pristine BFs in Figure 3a is smooth and with few defects. With the increase of seawater soaking time, the surface corrosion of BFs becomes more serious. The outside surface of BFs starts with the ‘point-like’ corrosion which is shown in Figure 3b, and gradually diffuses to the inside of the fiber and forms a ‘petal-like’ corrosion morphology shown in Figure 3c. Moreover, some fiber materials were peeled off from the BFs which is observed in Figure 2b. Lastly, the surface of BFs in Figure 3f is becoming similar to that in Figure 3b after 168 h of soaking.



**Figure 3.** Scanning electron microscopy (SEM) surface morphology of basalt fiber after immersing in seawater solution at 85 °C (a) pristine; (b) 6 h; (c) 12 h; (d) 18 h; (e) 24 h; (f) 168 h.

The EDS analysis of each BF was carried out by selecting a point on the surface (inside the red box), and the results are listed in Figure 4. Results show that most of the elements only have very minor change (<2 wt%) at the first 18 h, whereas MgO owns the biggest change around 4 wt%. With the corrosion proceeding, SiO<sub>2</sub> decreased around 3 wt% when the soaking time increased to 168 h, which indicates the damage of the former glass network.



**Figure 4.** Energy-dispersive X-ray spectroscopy (EDS) analysis of basalt fiber surface after soaking in 85 °C seawater solution for different times (wt%). Dash lines are the guide of eyes.

### 3.4. Microstructure (Fourier Transform Infrared (FT-IR) Spectroscopy)

To explore the glass microstructure, the FT-IR spectra of BFs after immersing them in seawater solution at 85 °C for different periods are shown in Figure 5. It can be seen that the peak wavenumber on the right side decreases from 1041  $\text{cm}^{-1}$  to 1085  $\text{cm}^{-1}$  which is corresponding to pristine BFs and BFs after soaking for 168 h. It is widely accepted that the FT-IR peak near 1050  $\text{cm}^{-1}$  represents the antisymmetric stretching vibration of Si-O-Si [24,25]. Thus, this corresponding peak shifts to higher wavenumbers with prolonging of soaking time. On the other hand, the peak at around 3433  $\text{cm}^{-1}$  does not change significantly which is associated with the O-H stretching vibration peak in -OH [26].

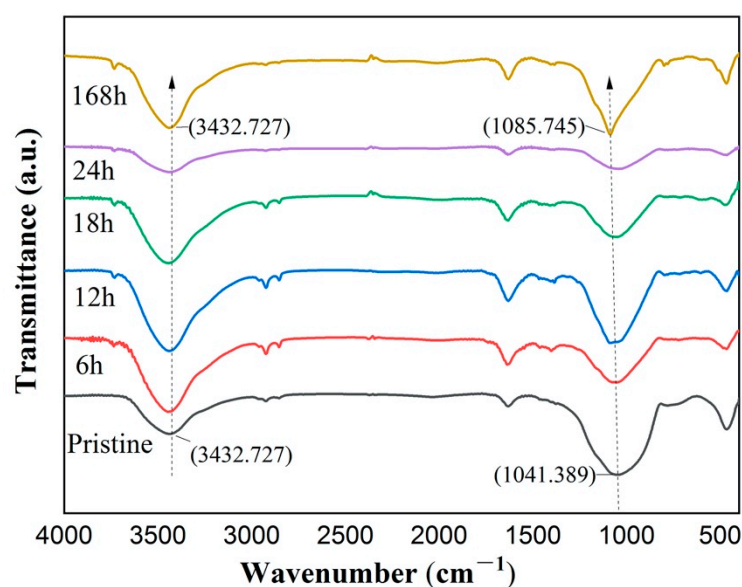


**Figure 5.** Fourier transform infrared (FT-IR) spectra of basalt fibers after being immersed in seawater solution at 85 °C for different times.

## 4. Discussion

What happened to the BFs during the first stage (around 18 h) of soaking? The weight-loss ratio decreased and the tensile strength increased after the first stage of soaking. The

surface morphology presents a severe surface corrosion structure including cavities and peelings. Meanwhile, MgO has a significant increase after soaking in seawater for around 18 h. We believe all those phenomena are related to each other.

Micro-crack theory [27] suggests that many tiny cracks or defects are always presented on glass surface. With the proceeding of corrosion (external stress), stress concentration will occur near those cracks and defects, and those cracks will propagate until fracture. Figure 6 describes the mechanism of the micro-crack blunting process [28]. First, microcracks always possess the weakest structure which provides ‘shortcuts’ and promotes the corrosion process (Figure 6a). This will lead to an increase in the weight-loss ratio and the decrease of the tensile strength of BFs. However, the corrosion process provides opportunities for ion exchange between the glass matrix and the seawater solution. One promising piece of evidence is the significant increase in MgO. The ion-exchange process will destroy the tip of microcracks (Figure 6c), which will lead to the blunting of microcracks (Figure 6d). Thus, the micro-crack blunting mechanism is the main reason for the decrease of weight-loss ratio and the increase of tensile strength at the first stage of soaking.

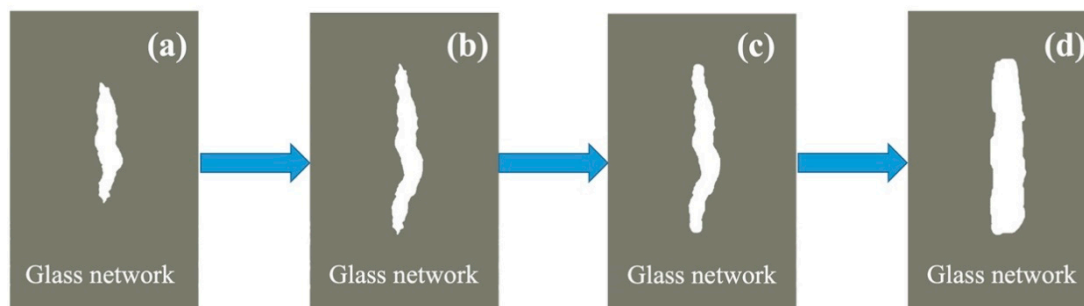


**Figure 6.** Schematic diagram of the micro-crack blunting mechanism (a) pristine; (b) microcracks growth; (c) tip of microcracks destroyed; (d) microcracks blunting.

Moreover, the FT-IR results show that, the Si–O–Si antisymmetric stretching vibration peak shifted to the higher wavenumbers with the increase of corrosion time, which represents the depolymerization [29,30] of the Si–O–Si tetrahedral structure. This is direct evidence to support, even the rigid glass network, e.g., Si–O–Si tetrahedral, was also slightly damaged during the corrosion process. The EDS analysis is also in agreement with this conclusion. However, the micro-crack blunting effect is more pronounced than the structure depolymerization at the first stage of soaking (around 18 h), which dominates the tensile strength of BFs.

We note that all the experiments were performed in an accelerated aging method [31,32] which was at a temperature higher than the true seawater environment. Nevertheless, the whole corrosion process at true seawater environment will be the same trend but much slower corrosion rate. Moreover, the mechanism of BFs destruction could be significantly different in different concretes, thus, more chemical and mechanical tests are needed in the future especially for BF composites in seawater environments.

## 5. Conclusions

The effect of seawater environment on chemical durability and tensile strength of basalt continuous fibers was investigated in this work. The main conclusions can be summarized as: (1) the weight-loss ratio of basalt fiber decreases at the first stage (around 18 h) of soaking at 80 °C, 85 °C, and 90 °C and then increases for longer soaking durations; (2) the tensile strength of basalt fiber undergoes the opposite change, which is an increase at the first stage and a decrease later at the same experimental conditions; (3) the enhancement of tensile strength and chemical resistance at the first stage of seawater soaking is due to the ion-exchange induced ‘blunting’ mechanism; (4) the FT-IR and EDS results revealed damage to the Si–O–Si tetrahedral structure during the corrosion process; however, the ‘blunting’ effect dominates the first stage.

**Author Contributions:** Conceptualization, Q.W.; methodology, L.D.; software, T.Y. and L.D.; validation, Q.W, T.Y. and L.D.; formal analysis, T.Y. and Q.W.; investigation, L.D.; resources, Q.W. and L.D.; data curation, T.Y.; writing—original draft preparation, L.D. and Q.W.; writing—review and editing, L.D.; visualization, T.Y. and L.D.; supervision, Q.W.; funding acquisition, Q.W. and L.D. All authors have read and agreed to the published version of the manuscript.

**Funding:** This study was funded by the National Science Foundation of China (NSFC, No. 51873032), the Fundamental Research Funds for the Central Universities (223201900003, 2232021D-04), the Key Research and Development Program of Shandong Province (2019JZZY010308), and the Open Fund of the State Key Laboratory of Luminescent Materials and Devices (South China University of Technology).

**Institutional Review Board Statement:** Not applicable.

**Informed Consent Statement:** Not applicable.

**Data Availability Statement:** The data presented in this study are available on request from the corresponding author.

**Conflicts of Interest:** The authors declare that they have no conflict of interest.

## References

1. Xing, D.; Xi, X.-Y.; Qi, M.-G.; Zheng, Q.-B.; Ma, P.-C. Optimization on the formulation of sizing to enhance the mechanical properties of basalt fiber. *J. Text. Inst.* **2021**, *112*, 515–525. [[CrossRef](#)]
2. Chen, M.; Liu, J.; Wu, Z. Effect of Fe<sub>2</sub>O<sub>3</sub> Concentration on the Properties of Basalt Glasses. *J. Nat. Fibers* **2020**, 1–11. [[CrossRef](#)]
3. Chen, X.; Zhang, Y.; Huo, H.; Wu, Z. Improving the tensile strength of continuous basalt fiber by mixing basalts. *Fibers Polym.* **2017**, *18*, 1796–1803. [[CrossRef](#)]
4. Chen, X.; Zhang, Y.; Huo, H.; Wu, Z. Study of high tensile strength of natural continuous basalt fibers. *J. Nat. Fibers* **2018**, *17*, 214–222. [[CrossRef](#)]
5. Sarasini, F.; Tirillo, J.; Seghini, M.C. Influence of thermal conditioning on tensile behaviour of single basalt fibres. *Compos. Part B Eng.* **2018**, *132*, 77–86. [[CrossRef](#)]
6. Jamshaid, H. Basalt Fiber and its Applications. *J. Text. Eng. Fash. Technol.* **2017**, *1*, 1–3. [[CrossRef](#)]
7. Afroz, M.; Patnaikuni, I.; Venkatesan, S. Chemical durability and performance of modified basalt fiber in concrete medium. *Constr. Build. Mater.* **2017**, *154*, 191–203. [[CrossRef](#)]
8. Sun, X.; Gao, Z.; Cao, P.; Zhou, C. Mechanical properties tests and multiscale numerical simulations for basalt fiber reinforced concrete. *Constr. Build. Mater.* **2019**, *202*, 58–72. [[CrossRef](#)]
9. Wang, X.; Zhao, X.; Wu, Z. Fatigue degradation and life prediction of basalt fiber-reinforced polymer composites after saltwater corrosion. *Mater. Des.* **2019**, *163*, 107529. [[CrossRef](#)]
10. Dong, Z.; Wu, G.; Xu, B.; Wang, X.; Taerwe, L. Bond durability of BFRP bars embedded in concrete under seawater conditions and the long-term bond strength prediction. *Mater. Des.* **2016**, *92*, 552–562. [[CrossRef](#)]
11. Xiong, Z.; Wei, W.; He, S.; Liu, F.; Luo, H.; Li, L. Dynamic bond behaviour of fibre-wrapped basalt fibre-reinforced polymer bars embedded in sea sand and recycled aggregate concrete under high-strain rate pull-out tests. *Constr. Build. Mater.* **2021**, *276*, 122195. [[CrossRef](#)]
12. Li, C.; Gao, D.; Wang, Y.; Tang, J. Effect of high temperature on the bond performance between basalt fibre reinforced polymer (BFRP) bars and concrete. *Constr. Build. Mater.* **2017**, *141*, 44–51. [[CrossRef](#)]
13. Sharma, S.; Zhang, D.; Zhao, Q. Degradation of basalt fiber-reinforced polymer bars in seawater and sea sand concrete environment. *Adv. Mech. Eng.* **2020**, *12*, 1687814020912888. [[CrossRef](#)]
14. Bazli, M.; Li, Y.-L.; Zhao, X.-L.; Raman, R.S.; Bai, Y.; Al-Saadi, S.; Haque, A. Durability of seawater and sea sand concrete filled filament wound FRP tubes under seawater environments. *Compos. Part B Eng.* **2020**, *202*, 108409. [[CrossRef](#)]
15. Lu, Z.; Xie, J.; Zhang, H.; Li, J. Long-Term Durability of Basalt Fiber-Reinforced Polymer (BFRP) Sheets and the Epoxy Resin Matrix under a Wet–Dry Cyclic Condition in a Chloride-Containing Environment. *Polymers* **2017**, *9*, 652. [[CrossRef](#)] [[PubMed](#)]
16. Lu, Z.; Su, L.; Tan, S.; Li, Y.; Xie, J.; Liu, F. Long-term shear performance of bare and cement mortar-coated BFRP bars in corrosive environments. *Constr. Build. Mater.* **2020**, *237*, 117658. [[CrossRef](#)]
17. Kim, D.; Mittal, G.; Kim, M.; Kim, S.; Rhee, K.Y. Surface modification of MMT and its effect on fatigue and fracture behavior of basalt/epoxy based composites in a seawater environment. *Appl. Surf. Sci.* **2019**, *473*, 55–58. [[CrossRef](#)]
18. Ulus, H.; Kaybal, H.B.; Eskizeybek, V.; Avci, A. Halloysite nanotube reinforcement endows ameliorated fracture resistance of seawater aged basalt/epoxy composites. *J. Compos. Mater.* **2020**, *54*, 2761–2779. [[CrossRef](#)]
19. Sethi, S.; Ray, B.C. Environmental effects on fibre reinforced polymeric composites: Evolving reasons and remarks on interfacial strength and stability. *Adv. Colloid Interface Sci.* **2015**, *217*, 43–67. [[CrossRef](#)]
20. Gutnikov, S.; Manylov, M.; Lipatov, Y.; Lazoryak, B.; Pokholok, K. Effect of the reduction treatment on the basalt continuous fiber crystallization properties. *J. Non Cryst. Solids* **2013**, *368*, 45–50. [[CrossRef](#)]

21. D 1141-98 (Reapproved 2013). In *Standard Practice for the Preparation of Substitute Ocean Water*; ASTM International: West Conshohocken, PA, USA, 2013.
22. Wang, Z.; Zhao, X.-L.; Xian, G.; Wu, G.; Raman, R.S.; Al-Saadi, S.; Haque, A. Long-term durability of basalt- and glass-fibre reinforced polymer (BFRP/GFRP) bars in seawater and sea sand concrete environment. *Constr. Build. Mater.* **2017**, *139*, 467–489. [[CrossRef](#)]
23. *BS ISO 11566:1996 Method B: Carbon fibre: Determination of the Tensile Properties of as Single-filament Specimens*; International Organization for Standardization: Geneva, Switzerland, 1996.
24. Kapeluszna, E.; Kotwica, L.; Różycka, A.; Gólek, L. Incorporation of Al in C-A-S-H gels with various Ca/Si and Al/Si ratio: Microstructural and structural characteristics with DTA/TG, XRD, FTIR and TEM analysis. *Constr. Build. Mater.* **2017**, *155*, 643–653. [[CrossRef](#)]
25. Ahlawat, R. Effect of Concentration and Temperature on the Surface morphology of Gd<sub>2</sub>O<sub>3</sub> Nanocrystallites in Silica. *Int. J. Appl. Ceram. Technol.* **2014**, *12*, 1131–1139. [[CrossRef](#)]
26. Ovchinnikov, O.V.; Evtukhova, A.V.; Kondratenko, T.S.; Smirnov, M.S.; Khokhlov, V.Y.; Erina, O.V. Manifestation of intermolecular interactions in FTIR spectra of methylene blue molecules. *Vib. Spectrosc.* **2016**, *86*, 181–189. [[CrossRef](#)]
27. Basoglu, M.F.; Zerín, Z.; Kefal, A.; Oterkus, E. A computational model of peridynamic theory for deflecting behavior of crack propagation with micro-cracks. *Comput. Mater. Sci.* **2019**, *162*, 33–46. [[CrossRef](#)]
28. Scudino, S.; Shahid, R.N.; Escher, B.; Stoica, M.; Li, B.S.; Kruzic, J.J. Mapping the cyclic plastic zone to elucidate the mechanisms of crack tip deformation in bulk metallic glasses. *Appl. Phys. Lett.* **2017**, *110*, 081903. [[CrossRef](#)]
29. Rao, T.; Kumar, A.R.; Rao, B.H.; Veeraiah, N.; Reddy, M.R. Optical absorption, ESR, FT-IR spectral studies of iron ions in lead oxyfluoro silicate glasses. *J. Mol. Struct.* **2012**, *1021*, 7–12. [[CrossRef](#)]
30. Piscicella, P.; Pelino, M. FTIR spectroscopy investigation of the crystallisation process in an iron rich glass. *J. Eur. Ceram. Soc.* **2005**, *25*, 1855–1861. [[CrossRef](#)]
31. Morales, C.N.; Claire, G.; Empananza, A.R.; Nanni, A. Durability of GFRP reinforcing bars in seawater concrete. *Constr. Build. Mater.* **2021**, *270*, 121492. [[CrossRef](#)]
32. Tu, J.; Xie, H.; Gao, K. Prediction of the Long-Term Performance and Durability of GFRP Bars under the Combined Effect of a Sustained Load and Severe Environments. *Materials* **2020**, *13*, 2341. [[CrossRef](#)]